Effect of Surfactant Solutions on the Drag and the Flow Pattern of a Circular Cylinder

Satoshi Ogata, Yoshihisa Osano, and Keizo Watanabe
Dept. of Mechanical Engineering, Tokyo Metropolitan University, Tokyo 192-0397, Japan

DOI 10.1002/aic.10595
Published online September 1, 2005 in Wiley InterScience (www.interscience.wiley.com).

The effect of surfactant solutions on the flow past a circular cylinder was investigated in the Reynolds number (Re) ranging between 10 and 10^5 by measuring the drag and by flow visualization. Surfactant solutions were aqueous solutions of oleyl-bihydroxyethyl-methyl-ammonium-chloride in the concentration range of 50 to 200 ppm, to which sodium salicylate was added as a counterion. It was clarified that the drag coefficient of the cylinder in surfactant solutions increases, comparing that in water in a lower Re range for constant cylinder diameter. On the contrary, the drag coefficient decreases in higher Re range. The Re range in which drag reduction occurs increases with increasing diameter. The flow visualization results show that the drag increases because of the existence of the wide stagnation zone around the cylinder. This zone disappears in the Re range in which drag reduction occurs. In this case, the separation point moves rearward and the velocity defect in the wake becomes smaller. © 2005 American Institute of Chemical Engineers *AIChE J,* 52: 49–57, 2006
Keywords: fluid mechanics and transport phenomena, external flow, circular cylinder, flow visualization, drag coefficient, surfactant solution

Introduction

Certain cationic surfactant solutions can reduce turbulent friction in pipe/channel flows. This drag reduction has attracted considerable attention from the perspective of energy conservation because mechanical degradation does not occur and the drag reduction ratio is higher than that in polymer solutions in certain concentration ranges.[1,2] Therefore, recently, surfactant has been added to the heating medium used for district thermal energy supply pipeline systems, and research on reducing the pumping power of the system has been performed.[3] With respect to the pressure loss in the pipeline, many studies have been conducted on the drag reduction by surfactant solutions for internal flows.[4-6]

Generally, at low shear rates the surfactant solutions are slightly shear thinning and the micelles become more aligned in the flow direction; as a result the shear viscosity increases suddenly and the solution is characterized as viscoelastic. This larger superordered structure of the aligned micelles is referred to as the *shear-induced state* (SIS). Drag-reducing surfactant solutions generally have strong viscoelasticity, so that viscoelasticity is considered to play an important role in the drag-reduction effect. However, Lin et al.[7] investigated the pipe flow of surfactant solutions (Arquad 16-50: cetyltrimethyl ammonium chloride, Ethoquad O/12™: oleyl-bihydroxyethyl-methyl-ammonium-chloride) with excess addition of counterions (NaSal), and reported that the turbulent drag reduction is also shown by surfactant solutions that do not show viscoelasticity. Considering that the drag-reducing surfactant solutions do not always have viscoelasticity as mentioned above, there are many unclear details for the relationship between the viscoelasticity and the drag reduction of surfactant solution at present.

On the other hand, by studying the flow past a circular cylinder, the effects of flow separation and wake on the drag of cylinder can be examined. In addition, such flow is related to the shear flow, which produces the shear-induced state, as mentioned above. Therefore, to clarify the effect of the shear-induced state on the flow characteristics and to examine the

mechanism of drag reduction, the flow of a cylinder in drag-reducing solutions should be investigated.

For drag-reducing polymer solutions, James and Acosta[8] measured the drag of cylinder in a dilute polymer solution (polyethylene oxide, WSR-205, WSR-301) in the Reynolds number (Re) < 50 region and clarified that the drag coefficient is independent of the uniform velocity and becomes constant above the critical uniform velocity, and that the drag coefficient is one order higher than that of water. Koniuta et al.[9] indicated these phenomena are caused by the existence of a wide stagnation zone around the cylinder. Marero and Mena[10] also showed that this zone becomes 10 times wider than that for water and occurred when the Deborah number (De) reaches 1.

Usui et al.[11] reported that the Strouhal number decreases at $50 < Re < 10^2$ by the use of a polymer solution [polyethylene oxide (PEO)]. In contrast, no difference was found[12,13] between the Strouhal number of polymer solutions and that of water at $10^2 < Re < 10^4$. In the case of the $Re > 10^4$, Turgut et al.[12] conducted an experiment involving a dilute polymer solution (polyethylene oxide, WSR-301) at $5 \times 10^4 < Re < 3 \times 10^5$ and found a drag reduction for the circular cylinder. They showed that the decrease in drag was attributed to the reduction in the size of the wake. The strong destabilizing effect of the additives on the vortex breakdown is also described. A similar study by Luikov et al.[14] has shown that the drag reduction is partly the result of a change in the characteristics of the vortex motion behind the cylinder.

With respect to the surfactant solutions, however, few studies have examined the flow around a circular cylinder. Research on surfactant solutions in an external flow is difficult because of bubble formation and complicated rheological behavior. Bergin et al.[15] investigated the flow past a circular cylinder in dilute surfactant solutions (tetradecyl trimethyl ammonium bromide with sodium salicylate, TTAB + NaSal) at $10^2 < Re < 2 \times 10^3$ by laser Doppler velocimetry (LDV) measurements and by visualization. They showed that the frequency of the vortex shedding of surfactant solutions decreases at $2 \times 10^2 < Re < 2 \times 10^3$, and that the flow pattern became smooth when a the shear-induced state was formed. They also showed that the streamwise components of the turbulent velocity fluctuations in dilute surfactant solutions were greater than those in tap water, whereas the tangential components were reduced dramatically. However, they did not measure the drag of the cylinder, and the relationship between the flow pattern and the drag is not known at present.

The purpose of this study is to clarify the effect of the drag-reducing surfactant additives on the flow characteristics around the cylinder at $10 < Re < 10^5$ by measuring the drag and by visualizing the flow experimentally.

Experimental Apparatus and Method

The test fluids were tap water and aqueous solutions of oleyl-bihydroxyethyl methyl ammonium chloride [$C_{18}H_{35}N(C_2H_4OH)_2CH_3Cl$, trade name: Ethoquad O/12™] at concentrations of 50, 100, and 200 ppm. Sodium salicylate (NaSal) was added as a counterion. The concentration ratio of counterion to surfactant was set at a molar ratio of 1:1.

The viscosity of the surfactant solutions was measured using a capillary viscometer, and the data are presented in Figure 1. The curve of the FENE-P model used in the simulation is also shown in Figure 1. The shear viscosity increases with solution concentration and decreases with shear rate. However, the shear viscosity tends to be constant in the high shear rate region. The viscosity differed with the type of viscometer,[16] and the hysteresis of the viscosity occurred when using a cone–plate viscometer.[17] In addition, Usui et al.[18] reported that, in the high shear rate region, the viscosity of surfactant solutions is approximately equal to that of tap water. Because the viscosity of surfactant solutions is dependent on several parameters, the Reynolds number was calculated based on the viscosity of tap water.

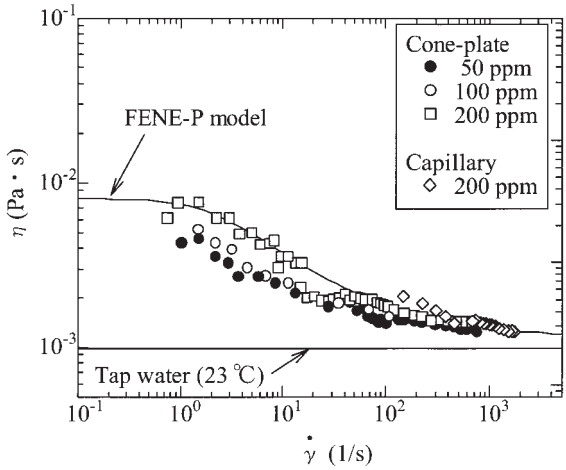

Figure 1. Shear viscosity of surfactant solution.

Figure 2 shows the experimental apparatus used for drag measurement at $10 < Re < 2 \times 10^2$. Figure 2a shows a detailed illustration of the drag detection unit, which can directly measure the drag acting on the circular cylinder. The test cylinder, having a diameter of 2 mm, was fixed on a flat plate in a vertical position. The flat plate was suspended horizontally by two leaf springs. The leaf spring is made of phosphor bronze [0.05 × 74 × 15 mm (thickness × length × width)]. The flat plate was slightly displaced in a direction perpendicular to the axis of the cylinder when the drag force acted on the cylinder. This small displacement was detected by a laser displacement sensor and was converted into the drag using the calibration factor of the leaf springs. The drag detection unit was calibrated by applying a known static load of the weight to the cylinder, and nonlinearly the error was 0.35%. Figure 2b shows a schematic diagram of the apparatus. The circular towing tank was made of stainless steel [860, 1080, 90 mm (ID, OD, depth, respectively)]. The drag-detection unit and the test cylinder were mounted on the rotating arm, and moved in the circular towing tank filled with the test fluids. The rotational speed was adjusted by controlling the motor unit.

For the $2 \times 10^2 < Re < 10^5$ region, the experiments were performed in a vertical recirculating water tunnel equipped with a clear plastic test section [298 × 250 × 1190 mm (width × height × length)]. In the water tunnel, the combination of a motor with continuously variable speed and a pump circulated the fluid at test section velocities ranging up to 1.2 m/s.

Figure 3 shows the experimental apparatus used for drag measurement at $2 \times 10^2 < Re < 7 \times 10^3$. The flat plate was

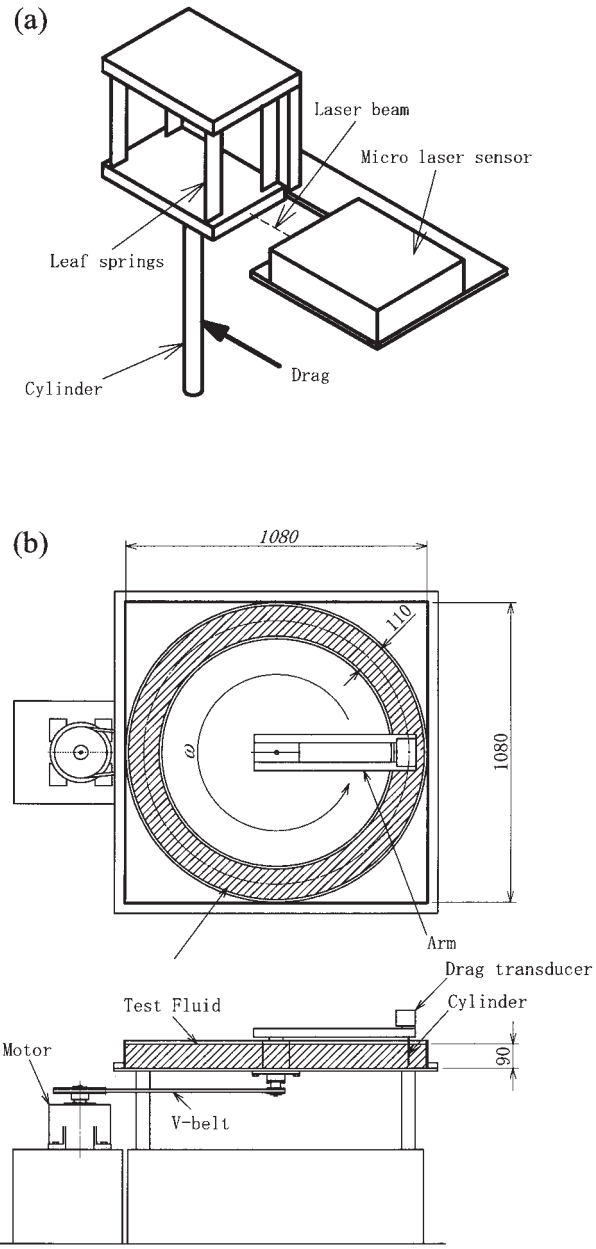

Figure 2. Experimental apparatus for $10 < Re < 2\times10^2$.

(a) Detailed illustration of the drag transducer; (b) Towing circular tank and schematic diagram of the experimental setup. Measurements given in mm.

suspended by four sufficiently long wires at each of the four corners. The measurement of the drag of the test cylinder was performed using a small load cell. The diameters of the test cylinders were $d = 5$, 7, 10, 13, and 20 mm. The load sensor of the load cell was fixed directly to the top of the cylinder to reduce the effect of cylinder vibration on the measurement. The experimental apparatus was calibrated in a manner similar to that in Figure 2a; the relationship between the known static load and the output from the load cell showed the linear relationship in the region > 3 mN, and the linearity error was 0.9%.

The cylinders with $d = 20$, 35, and 50 mm, extending through both tunnel walls, were used for the pressure measurement and the measurement of the velocity of the wake at $10^4 < Re < 10^5$. The pressure distribution around the cylinder was measured by means of a pressure transducer. A static pressure hole of diameter 0.5 mm was located at a distance 400 mm upstream of the cylinder. A pressure hole of diameter 0.5 mm was bored through the cylinder surface at a point midway along the length of the cylinder and was connected to a pressure transducer from the upper side of the cylinder. The local pressure on the cylinder surface was measured at 5 ° intervals. The drag coefficient C_d of cylinder was obtained by integrating the pressure coefficient, expressed as

$$C_d = \frac{2D}{d\rho U_m^2} = \int_0^{\pi} C_p \cos\phi d\phi \tag{1}$$

To measure the velocity behind the cylinder, a hot-film probe was positioned downstream at the half-length of the cylinder. Measurements were made at seven downstream positions: $x = 30$, 60, 90, 120, 150, 180, and 210 mm, and at 25 traverse stations behind the test cylinder. James and Acosta[8] reported that calibration of the hot-film probe is necessary when used in a dilute polymer solution because of the influence of polymer additives on the probe. The calibration also appears to be necessary for the probe when used in the surfactant solution. Therefore, the correlation between the experimental data for tap water and data for surfactant solutions is thought to require some correction. The calibration of the hot-film probe was performed directly using the steady rotating channel flow of surfactant solutions at the same concentration and temperature. In addition, the drag coefficient was calculated based on the velocity defect for comparison with that obtained based on the pressure distribution (Eq. 1). The total drag of the cylinder in two-dimensional flow can be calculated by the weighing

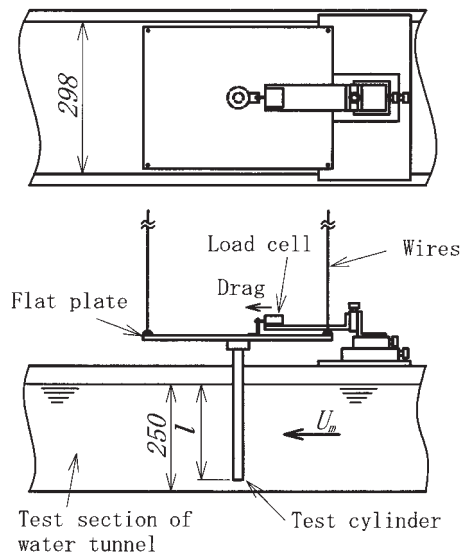

Figure 3. Experimental apparatus for $2 \times 10^2 < Re < 7 \times 10^3$.

Measurements given in mm.

Table 1. Dimensions of Test Cylinders and Methods of Drag Measurement

	Reynolds Number Range					
	$10 < Re < 2 \times 10^2$		$2 \times 10^2 < Re < 7 \times 10^3$		$10^4 < Re < 10^5$	
	d	l/d	d	l/d	d	l/d
Dimensions of test cylinders	2	45				
			5	12 24 48		
			7	12 24		
			10	12 24		
			13	12		
			20	12	20	∞
					35	∞
					50	∞
Method of drag measurement	Direct		Direct		Calculation from pressure distribution and velocity profiles	

lacks of velocity profiles. The total drag per unit length on the circular cylinder D is given as follows

$$D = \rho \int_{-\infty}^{+\infty} U(U_m - U)dy \tag{2}$$

Table 1 shows the dimensions of the test circular cylinder. All cylinders were made of stainless steel, and the surfaces and end faces of the cylinders were finished to sufficient smoothness.

In addition, we visualized the flow around the cylinders to clarify the relationship between the drag and the flow pattern past a circular cylinder. The test cylinders had $d = 2$ and 20 mm. For the cylinder with $d = 2$ mm, the visualization was performed using the laser-induced fluorescence technique. In place of the drag-detection unit shown in Figure 2, a digital video camera was placed on the arm. For the cylinder with $d = 20$ mm, the flow was visualized by a water-based dye injected upstream of the cylinder, which was placed in the test section of the recirculating water tunnel.

Results and Discussion

Figure 4 shows the experimental results for the drag coefficients in surfactant solutions and tap water, respectively. For comparison, the experimental results for a Newtonian fluid with $(l/d) = 5$ and ∞ obtained by Wieselsberger[19] are also shown in this figure. The drag coefficient from the velocity profiles and that from the pressure distribution agree within approximately 3.5% for both tap water and surfactant solutions. The results for the drag coefficient in tap water agree well with Wieselsberger's data. For tap water, therefore, it can be considered that there are few effects of the flow geometry and the experimental methods on the drag coefficient.

On the other hand, the drag coefficients of surfactant solutions are significantly different from that of water, and the data are significantly dependent on the cylinder diameter in Figure 4.

For the cylinder with $d = 20$ mm, the drag coefficient was higher than that of tap water at $10^3 < Re < 3 \times 10^3$ for 200 ppm surfactant solution. The drag coefficient decreased with increasing Reynolds number, and the slope of the curve of the drag coefficient increased with the concentration. When the Reynolds number reached approximately 3×10^3, the drag coefficient decreased compared to that of tap water. In other words, drag reduction occurred in this Reynolds number range. The maximum drag reduction rate reached 55% at $Re = 7 \times 10^3$ in 200 ppm surfactant solution. The onset Reynolds number of drag reduction was almost the same, regardless of the concentration. The drag coefficient decreased with increasing Reynolds number. When the Reynolds number increased further, the difference between the drag coefficient of the surfactant solution and that of water decreased and the drag reduction eventually vanished. These Reynolds number ranges are dependent on the cylinder diameter and decrease with decreasing the cylinder diameter.

In the case of the cylinder with $d = 2$ mm, the drag coefficient was one to three orders of magnitude higher than that of water at $10 < Re < 10^2$. This higher drag coefficient in the low Reynolds number range gradually decreases with increasing Reynolds number. The drag coefficient also increased with increasing surfactant concentration in this Reynolds number range. When the Reynolds number reaches approximately 10^2, the drag coefficient has an inflection point, after which the drag coefficient suddenly decreases and approaches the results

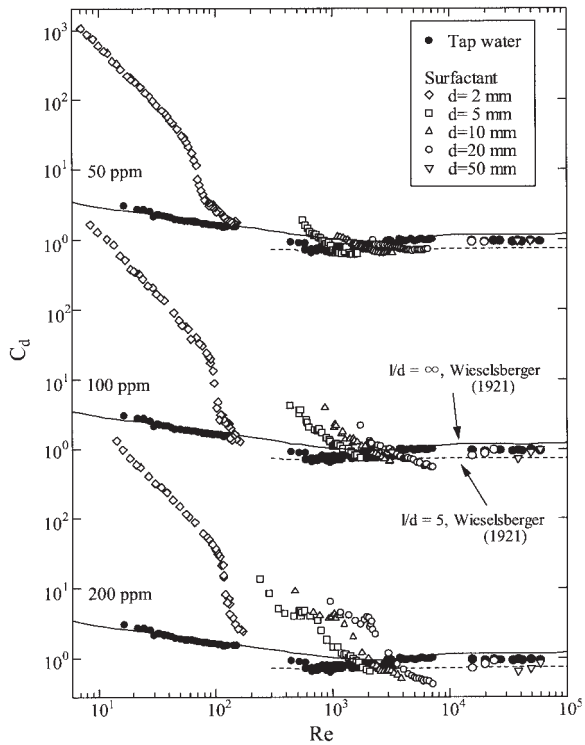

Figure 4. Drag coefficient of cylinder in surfactant solutions.

$(l/d) = 12$; for the cylinder with $d = 5$, 10, and 20 mm at $2 \times 10^2 < Re < 7 \times 10^3$.

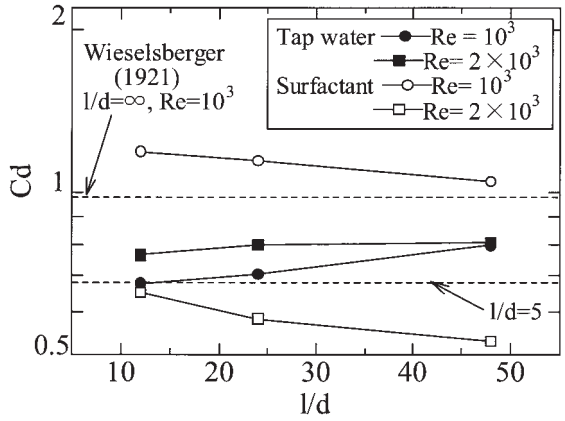

Figure 5. Effect of (*l*/*d*) on drag coefficient for *d* = 5 mm.

for tap water at $Re > 10^2$. These inflection points shifted to the high Reynolds number range with increasing cylinder diameter in 200 ppm surfactant solution.

Figure 5 shows the effect of (l/d) on the drag coefficients at $Re = 10^3$ and 2×10^3, respectively. For comparison, the experimental results for a Newtonian fluid with (l/d) = 5 and ∞ at $Re = 10^3$ are also shown in this figure.[19] In Figure 5, the drag coefficient of tap water decreases with decreasing (l/d), and the tendency of the data is the same as that of the previous experimental result for Newtonian fluid. In the case of surfactant solution, the drag coefficient decreased with increasing (l/d), different from the case of Newtonian fluid, because the flow condition that passed behind the cylinder through the cylinder end in surfactant solution could be different from that in tap water. However, the details of the flow condition are not known at present. Details of the condition will have to await clarification in future investigations.

Figure 6 shows the effect of the cylinder diameter at constant Reynolds number on the drag reduction ratio DR, which is defined by

$$\mathrm{DR}\ (\%) = \frac{C_d|_N - C_d|_S}{C_d|_N} \times 100 \qquad (3)$$

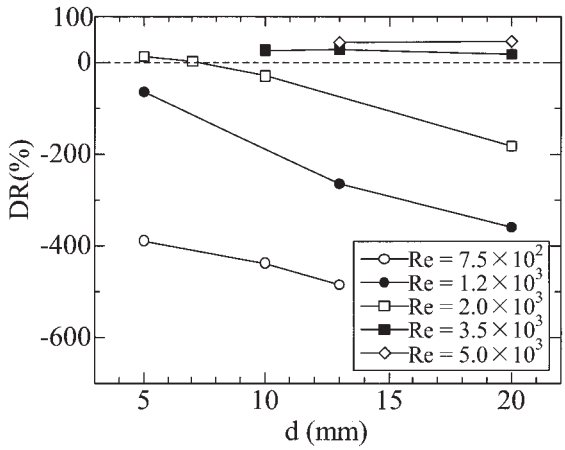

Figure 6. Effect of cylinder diameter on drag reduction in Ethoquad O/12 with 200 ppm.

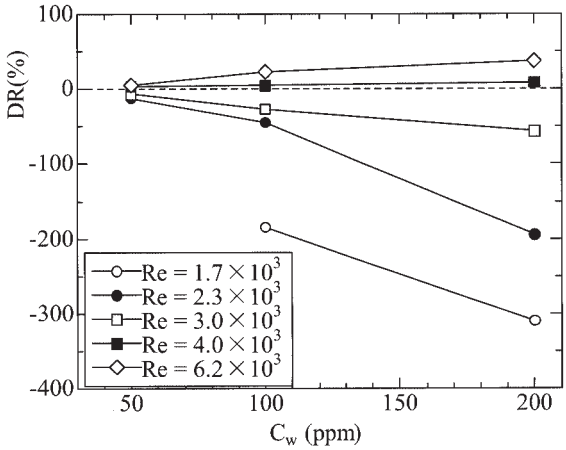

Figure 7. Effect of surfactant concentration on drag reduction for *d* = 20 mm.

where the subscripts S and N denote surfactant solution and tap water, respectively. It was clarified that DR decreases with increasing cylinder diameter for a small Reynolds number, and that the dependency on the diameter increases with decreasing Reynolds number. For a large Reynolds number, DR increases with increasing diameter.

Figure 7 shows the effect of the concentration of surfactant solution at constant Reynolds number on the drag reduction ratio. The drag reduction ratio decreases with increasing surfactant concentration in the case of either a small diameter or a small Reynolds number. The effect of the concentration on DR decreases with increasing Reynolds number. On the other hand, for a large Reynolds number DR increases with concentration. In other words, the increase in the concentration of the surfactant solution amplifies the characteristics of drag reduction or drag increase.

Figure 8 shows photographs of the flow around a cylinder of $d = 2$ and 20 mm in a 200 ppm surfactant solution, respectively. Generally, for Newtonian fluids, a twin vortex is formed at $10 < \mathrm{Re} < 50$ and the Kármán vortex street is generated in $\mathrm{Re} > 50$. In Figures 8a and 8d, the Kármán vortex is clearly observable in the case of tap water in this Reynolds number range.

For surfactant solutions, the flow pattern was significantly different from a Newtonian flow. In the case of the cylinder with $d = 2$ mm at $Re = 20$, at which the drag of the surfactant solution substantially increased, the low-velocity zone spreads widely upstream and over the cylinder surface (Figure 8b). This zone becomes 2.5 times the diameter in front and side of the cylinder, and 150 times the diameter streamwise direction, respectively. As the Reynolds number increased, this zone became narrower, until finally becoming nonexistent, and a smooth-flow pattern was observed (Figure 8c). In other words, the drag coefficient decreases with decreasing size of the low-velocity zone (Figure 4).

When the cylinder diameter is increased, a similar flow pattern is observed. For the cylinder with $d = 20$ mm, a wide stagnation zone exists around the cylinder at $Re = 2 \times 10^3$ (Figure 8e), at which the drag of the surfactant solution increases. As in the case of the cylinder with $d = 2$ mm, this zone finally became nonexistent and a smooth-flow pattern was

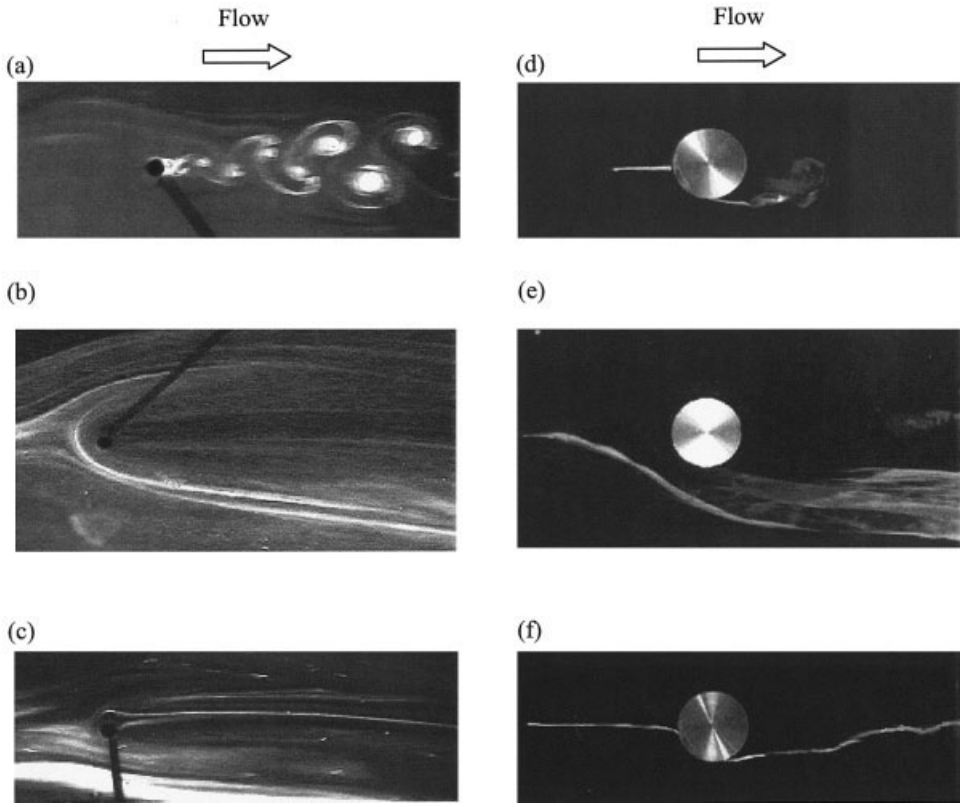

Figure 8. Flow past a cylinder with $d = 2$ and 20 mm, respectively.

(a) $d = 2$mm in tap water for $Re = 100$; (b) $d = 2$ mm in Ethoquad O/12 with 200 ppm for $Re = 20$; (c) $d = 2$ mm in Ethoquad O/12 with 200 ppm for $Re = 100$; (d) $d = 20$ mm in tap water for $Re = 10^4$; (e) $d = 20$ mm in Ethoquad O/12 with 200 ppm for $Re = 2000$; (f) $d = 20$ mm in Ethoquad O/12 with 200 ppm for $Re = 10^4$.

observed (Figure 8f), and the Kármán vortex street (see Figure 8d) was not found. For $d = 20$ mm, the width of the wake decreased compared with that of tap water for the Reynolds number at which drag reduction occurred. In addition, the point at which the flow separated can be also discerned from Figures 8d and 8f. Figure 8d shows that the angle of separation for tap water is approximately $\phi = 80°$, which is consistent with the experimental data from previous studies with Newtonian fluids.[20] Figure 8f shows that for surfactant solutions the separation point moves downstream. The separation angle is approximately $\phi = 110°$ in this case. An increase in the separation angle, arising from long-chain molecules, was also found by Brennen[21] and Turgut et al.[12]

To examine the factor of the spread of the stagnant area around the cylinder, the flow around the circular cylinder with $d = 2$ mm was simulated numerically. Here, we used the POLYFLOW (Fluent Inc., Lebanon, NH) finite-element-based simulation program and the FENE-P model.[22] The FENE-P model is a viscoelastic model, but the model cannot model the shear-induced structure (SIS). The calculation fluid is a viscoelastic fluid equivalent to 200 ppm Ethoquad O/12 ™ solutions with respect to physical properties of increased apparent shear viscosity, and the fitting curve of the FENE-P model is presented in Figure 1. Figure 9 shows the results of the numerical simulation for the Newtonian model and the FENE-P model around the cylinder, respectively. To show that the extent of the streamline of the FENE-P model is considerably wider than the Newton model, the scales of the two figures are different. For the Newtonian model, a twin vortex is formed in the wake (Figure 9a). For the FENE-P model, the low-velocity zone spreads widely upstream and over the surface of the cylinder (Figure 9b). The flow pattern of upstream of the cylinder agrees qualitatively with the results observed in flow visualization (Figure 8b), although it does not agree in the wake region. The numerical simulation result seems to indicate that the viscoelasticity, which related to the increased apparent shear viscosity, is one of the factors of the expansion of stagnation zone upstream of the cylinder.

The results of the velocity profiles of the wake and the pressure distribution around the cylinder at the Reynolds number, in which drag reduction occurs, are shown in Figures 10 and 11, respectively.

Figure 10 shows the experimental results of the traverse velocity profile at downstream stations of $x/d = 1.8$, 3.5, and 5.1 at $\mathrm{Re} = 10^4$. As seen in the figure, there is only a small difference between the wakes of the 50 ppm surfactant solution and tap water. However, for the 100 and 200 ppm surfactant solutions, the width of the velocity defect is smaller than that for tap water. The velocity profiles for surfactant solutions recovered to the mean velocity profiles earlier than did that for tap water. It is interesting that there is a local peak in the center of the velocity profile only for the 200 ppm data.

Figure 11 presents the pressure coefficients for the four test fluids at several Reynolds numbers. The dashed lines show the pressure coefficient under ideal flow conditions. The experimental results for $\mathrm{Re} = 6 \times 10^4$, given by Fage and Falkner,[23]

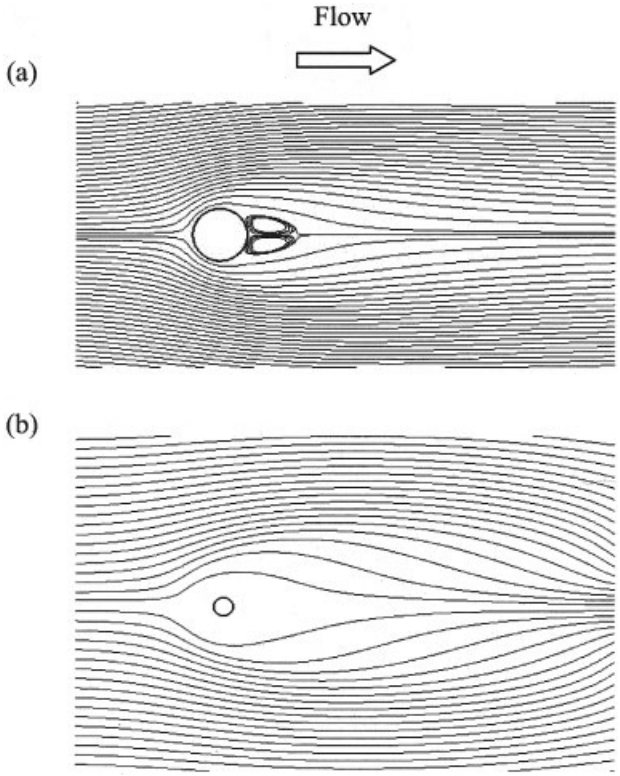

Figure 9. Numerical simulation results for the flow past a cylinder with d = 2 mm at Re = 20.

(a) Newtonian fluid model; (b) FENE-P model.

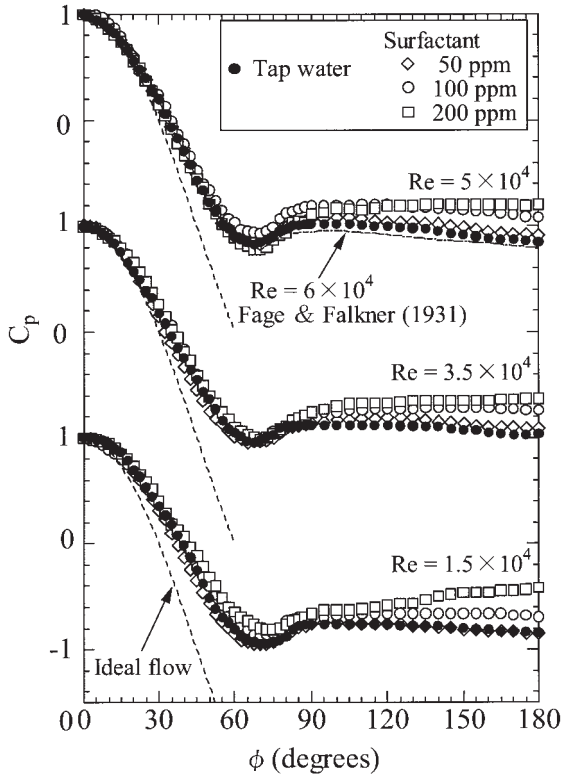

Figure 11. Pressure distributions of a circular cylinder.

are also indicated by a dotted line for comparison. The tap water data at $Re = 5 \times 10^4$ agree approximately with the experimental results of Fage and Falkner. There is a difference between the surfactant solution and tap water at higher Reynolds numbers, at which the drag reduction occurs, and the difference increases with Reynolds number. The pressure coefficients of the surfactant solution increase with concentration, especially toward the rear of the cylinder.

At lower Reynolds numbers, the drag of the cylinder increases compared to that of tap water because the wide stagnation area around the cylinder causes the cylinder diameter to virtually increase. The threadlike micelles in the surfactant solution are entangled and form the large network structure (SIS) under shear flow.[2] When the velocity of the flow around the cylinder is very low (or when Reynolds number is very small), the threadlike micelles seem to be entangled and accumulated in front of the cylinder, forming the SIS in the shear region near the cylinder. As indicated by the numerical simulation of Figure 9b, it can be considered that these phenomena depend on the viscoelasticity, which related to the generation of the SIS. With respect to the SIS, Lu et al.[24] confirmed that the micelles network structures exist even though shear is applied for only a very short time from their Cryo-TEM images of Ethoquad O/12 ™ solutions. In this study, the micelles network structures seem to be formed in the shear region of the cylinder.

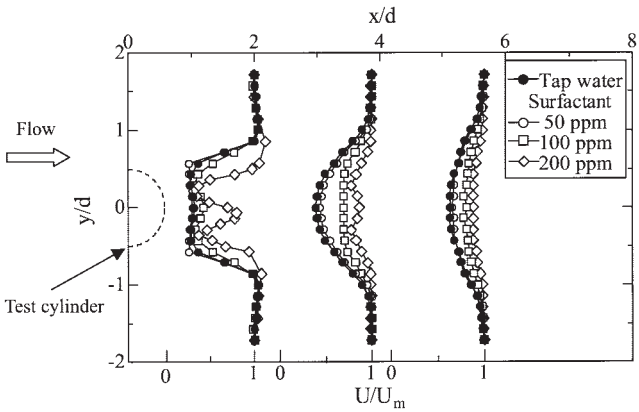

Figure 10. Velocity profiles in the wake of a cylinder with d = 35 mm at Re = 10^4.

At higher Reynolds numbers, the width of the wake of the surfactant solution is very narrow, so that the pressure difference between the front and rear of the cylinder decreases as mentioned in Figures 10 and 11. In other words, the drag reduction occurs as a result of the surfactant solution at higher Reynolds numbers ranges, at which the pressure drag makes up the greatest portion of the total drag. When the velocity increases and the force that works on the SIS increases as a result, the sedimentary layer around the cylinder seems to become thin because the local viscosity decreases with increasing shear rate. In addition, the effect of extensional flow in the wake of the cylinder seems to be intensified because of the increased elongational viscosity of the SIS.[25] The micelles network structure seems to be extended in the flow direction, so that the cylinder wake can be considered to become narrower and the separation point moves rearward.

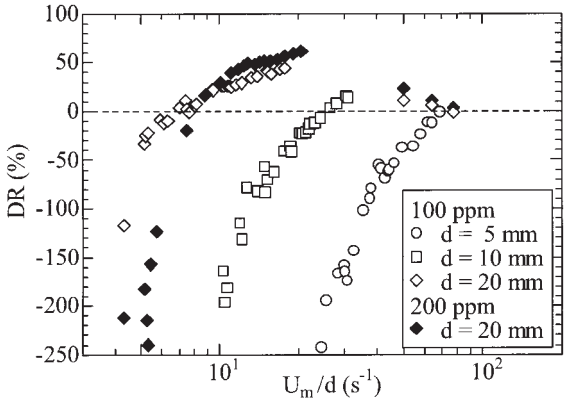

Figure 12. Effect of U_m/d on drag reduction ratio.

The results for the drag coefficient and the flow visualization show that the flow of the surfactant solution is dependent on the cylinder diameter and the mean velocity and that the flow pattern is closely related to the drag characteristics of the cylinder because the time in which the fluid has been accumulated in neighborhood of the cylinder and the deformation velocity of the fluid are dependent on flow velocity and diameter. In addition, the parameter U_m/d is related to the elongational viscosity of the solutions. Therefore, to clarify the effect of deformation rate (elongational strain rate) on the drag of the cylinder, the experimental results are rearranged using U_m/d.

Figure 12 shows the relationship between U_m/d and the drag reduction ratio. For the cylinder with $d = 20$ mm, drag reduction occurs when $8 < U_m/d < 60$. DR decreases with increasing U_m/d in the range of $U_m/d < 20$, and DR decreases with decreasing U_m/d in the range of $U_m/d > 50$. The onset and end Reynolds numbers of drag reduction are approximately the same, regardless of the concentration. Figure 12 also shows that the U_m/d at which drag reduction begins decreases with increasing cylinder diameter, and that the slope of the DR curve is independent of the diameter. This figure indicates that the drag of the cylinder in the surfactant solution cannot be discussed based only on U_m/d.

To clarify the characteristics of the drag coefficient and flow pattern in surfactant solution in greater detail, it is necessary not only to accumulate more data but also to establish the constitutive equation that can systematically express the viscoelastic property of a surfactant solution. Our drag data and flow visualization results are useful in establishing the constitutive equation of surfactant solutions.

Conclusions

The flow of surfactant solutions past a circular cylinder was investigated at $10 < Re < 10^5$. Experiments were carried out by measuring the drag and by visualizing the flow experimentally. The pressure distribution around the cylinder and the velocity profiles of the wake were also clarified. The following are the findings of the present study:

(1) The drag coefficient of surfactant solutions increases compared to that in tap water in the lower Reynolds number range. On the contrary, the drag coefficient decreases in the higher Reynolds number range. The Reynolds number range in which drag reduction occurs is dependent on the cylinder diameter. As a representative case, the drag coefficient of a cylinder with $d = 20$ mm increases compared to that of tap water at $10^3 < Re < 3 \times 10^3$. On the other hand, drag reduction occurs at $3 \times 10^3 < Re < 3 \times 10^4$, and the maximum drag reduction ratio was approximately 55% for the 200 ppm surfactant solution at $Re = 7 \times 10^3$.

(2) The increase in drag coefficient at lower Reynolds number was caused by the existence of a wide stagnation zone around the cylinder. The increased apparent shear viscosity of the surfactant solutions is a factor in the stagnation zone.

(3) The drag coefficient increased with increasing cylinder diameter with constant Reynolds number. The increase in the concentration of surfactant solution emphasized the characteristics of drag reduction and drag increase.

(4) When the drag reduction occurred, the stagnation zone disappeared. The separation point moved rearward and the width of the wake decreased. The drag reduction at higher Reynolds number was caused by the very narrow wake and the increased pressure at the rear of the cylinder.

Acknowledgments

We thank S. Matsuda and H. Kojima, undergraduate students at Tokyo Metropolitan University, for their help in performing the experiments. This research was supported by a Grant-in-Aid for the Encouragement of Young Scientists (B), No. 14750122, from the Scientific Research Fund of the Japanese Government.

Notation

C_d = drag coefficient of circular cylinder
C_p = pressure coefficient
C_w = concentration of surfactant solution
d = diameter of circular cylinder
DR = drag reduction ratio
l = length of circular cylinder
Re = Reynolds number ($=U_m d/\nu$)
U = velocity
U_m = mean velocity
x, y, z = Cartesian coordinates

Greek letters

$\dot{\gamma}$ = shear rate
η = viscosity of test solution
ν = kinematic viscosity of water
ρ = density of water

Literature Cited

1. Zakin JL, Chang JL. Polyoxyethylene alcohol non-ionic surfactants as drag reducing additives. In: Coles NG, ed. *Proceedings of the International Conference on Drag Reduction, 1974, at St John's College, Cambridge*. Vol. D1. Cranfield, Bedford, UK: BHRA Fluid Engineering; 1975:1-14.
2. Ohlendorf D, Interthal W, Hoffmann H. Surfactant systems for drag reduction: Physico-chemical properties and rheological behavior. *Rheol Acta.* 1986;25:468-486.
3. Gasljevic K, Matthys EF. Field test of a drag-reducing surfactant additive in a hydraulic cooling system. Proc of ASME Fluids Engineering Division Summer Meeting, San Diego, CA, July 7–11, FED-237; 1996:249-260.
4. Bewersdorff HW, Ohlendroff D. The behaviour of drag-reducing cationic surfactant solution. *Colloid Polym Sci.* 1988;266:941-953.
5. Warholic MD, Schmidt GM, Hanratty TJ. The influence of a drag-reducing surfactant on a turbulent velocity field. *J Fluid Mech.* 1999; 388:1-20.
6. Zakin JL, Myska J, Chara Z. New limiting drag reduction and velocity

profile asymptotes for nonpolymeric additives systems. *AIChE J.* 1996;42:3544-3546.
7. Lin Z, Zheng Y, Davis HT, Scriven LE, Talmon Y, Zakin JL. Unusual effects of counterion to surfactant concentration ratio on viscoelasticity of a cationic surfactant drag reducer. *J Non-Newtonian Fluid Mech.* 2000;93:363-373.
8. James DF, Acosta AJ. The laminar flow of dilute polymer solutions around circular cylinders. *J Fluid Mech.* 1970;42:269-288.
9. Koniuta A, Adler PM, Piau JM. Flow of dilute polymer solutions around circular cylinders. *J Non-Newtonian Fluid Mech.* 1980;7:101-106.
10. Manero O, Mena B. On the slow flow of viscoelastic liquids past a circular cylinder. *J Non-Newtonian Fluid Mech.* 1981;9:379-387.
11. Usui H, Shibata T, Sano Y. Kármán vortex behind a circular cylinder in dilute polymer solutions. *J Chem Eng Jpn.* 1980;13-1:77-79.
12. Turgut S, Rainey PG, Kell RE. Flow of dilute polymer solutions about circular cylinders. *J Fluid Mech.* 1973;57:177-208.
13. Kim BK, Telionis DP. The effect of polymer additives on laminar separation. *Phys Fluids.* 1989;A1:267-273.
14. Luikov AV, Shulman ZP, Puris BI. Mass transfer of a cylinder in forced flow of non-Newtonian viscoelastic fluid. *Heat Transfer Soviet Res.* 1969;1-1:121-132.
15. Bergins C, Nowak M, Urban M. The flow of a dilute cationic surfactant solution past a circular cylinder. *Exp Fluids.* 2001;30:410-417.
16. Bewersdorff HW. Rheology of drag reducing surfactant solutions. Proc of ASME Fluids Engineering Division Summer Meeting, San Diego, CA, July 7–11, FED-237; 1996;:25-29.
17. Wunderlich AM, Brunn PO. The complex rheological behavior of an aqueous cationic surfactant solution investigated in a Couette-type viscometer. *Colloid Polym Sci.* 1989;267:627-636.
18. Usui H, Ito T, Saeki T. Drag reducing pipe flow of surfactant solutions. Proc of ASME Fluids Engineering Division Summer Meeting, San Diego, CA, July 7–11, FED-237; 1996:159-163.
19. Wieselsberger C. Versuche über den Luftwiderstand gerundeter und kantiger Körper. *Ergebnisse der Aerodynamischen versuchsanstalt zu Göttingen*. Lieferung II; 1921.
20. Achenbach E. Distribution of local pressure and skin friction around a circular cylinder in cross-flow up to Re = 5×10^6. *J Fluid Mech.* 1968;34:625-639.
21. Brennen C. Some cavitation experiments with dilute polymer solutions. *J Fluid Mech.* 1970;44:51-63.
22. Bird RB, Armstrong RC, Hassenger O. *Dynamics of Polymeric Liquids 2*. 2nd Edition. New York, NY: Wiley; 1987.
23. Fage A, Falkner VM. Further experiments on the flow around a circular cylinder. Aeronautics Research Council (ARC) RM 1369 (Rep. and Mem., No. 1369); 1931.
24. Lu B, Zheng Y, Davis HT, Scriven LE, Talmon Y, Zakin JL. Effect of variations in counterion to surfactant ratio on rheology and microstructures of drag reducing cationic surfactant systems. *Rheol Acta.* 1998; 37:528-548.
25. Wunderlich AM, James DF. Extensional flow resistance of dilute polyacrylamide and surfactant solutions. *Rheol Acta.* 1987;26:522-540.

Manuscript received Sep. 2, 2004, and revision received May 6, 2005.